This article was published in Journal of Physical Chemistry Letters, 6(5), 845-851, 2015
http://dx.doi.org/10.1021/jz502380b

Modeling the Growth Kinetics of Anodic TiO_2 Nanotubes

A. Apolinário,† P. Quitério,† C. T. Sousa,† J. Ventura,† J. B. Sousa,† L. Andrade,‡ A. M. Mendes,‡ and J. P. Araújo*,†

†IFIMUP and IN-Institute of Nanoscience and Nanotechnology, Dep. de Física e Astronomia, Faculdade de Ciências da Universidade do Porto, Rua do Campo Alegre, 678, 4169-007 Porto, Portugal

‡LEPABE-Laboratory for Process Engineering, Environment, Biotechnology and Energy, Dep. Engenharia Química-Faculdade de Engenharia, R. Dr. Roberto Frias, 4200-465 Porto, Portugal

Abstract

The fundamental understanding of the barrier layer (δ_b) growth in TiO_2 nanotubes (NTs) is here established and compared with the classical metal oxidation theory from Mott and Cabrera. The role of δ_b in the anodization of TiO_2 NTs under different applied potentials and times was analyzed using scanning transmission electron microscopy (STEM). Contrary to the well-known case of anodic aluminum oxide, we found that δ_b of TiO_2 NTs progressively grows over time due to the nonsteady anodization regime. We then establish a relation between the phenomenological growth of the barrier layer with time and applied voltage, $\delta_b(V,t)$ using the high-field Mott and Cabrera conduction theory. The developed model was found to be in excellent agreement with the experimental data from both STEM and anodization curves. On the basis of these results, the relationship between δ_b and the anodization time and potential can now be quantitatively understood.

Theory of the oxidation of metals goes back to the late 1940s, when Mott and Cabrera discussed the growth of oxide thin films formed by anodic oxidation under an applied electric field.[1] In the Mott−Cabrera picture, the oxide growth of Ti and other valve metals (Al, Hf, Ta, W, etc.) is governed by the high-field conduction mechanism.[1−3] Under higher fields,

the entry of a cation across the metal/oxide interface into the oxide is the oxide growth rate-determining step. Thus, during oxidation, both the rate of oxidation and the rate-limiting process depend on the thickness of the oxide.[1] According to the underlying theory, the growth kinetics of the passive film is described by the relation between current density (j) and the electric field strength ($E = V/\delta_b$, where V is the applied potential and δ_b the oxide thickness)

$$j = \alpha\, e^{\beta E} \ldots \qquad (1)$$

Under this approach, the electrochemical oxidation of metals can lead to (i) stable continuous oxide

films, if the oxide is insoluble to the electrolyte, or (ii) nanoporous oxide films if the oxide is fairly soluble in the presence of an acidic electrolyte.[4] Indeed, in past decades, Al and Ti electrochemical anodization together with other valve metals (Hf, Ta, W, etc.) has been widely studied because highly regular hexagonal arrangements of pores or nanotubes can be obtained. Both anodic aluminum oxide (AAO) nanoporous and anodic TiO_2 nanotubes (NTs) have stimulated considerable scientific and technological interest with extensive use in practical nanostructures.[5−9] In particular, the distinct properties of anodic TiO_2 NTs make it highly attractable for a wide range of applications, mainly in renewal energy sources such as H_2 generation by water photoelectrolysis and dye-sensitized solar cells (DSCs).[6,7]

Because Zwilling et al. first introduced the anodic oxidation of Ti using fluoride-based electrolytes,[10] anodization parameters such as electrolyte composition, applied potential, time, temperature, and Ti surface roughness were found to significantly influence the growth and morphology of TiO_2 NTs. This influence is seen in the crucial geometrical features of NTs: length, porosity, pore diameter, interpore distance, wall thickness, barrier layer thickness, array organization, and smoothness.[9,11−22]

In the anodization the growth of the barrier layer thickness (δ_b) at the NTs bottom is governed by the high-field conduction mechanism.[1−3] While the highly studied AAO presents a steady-state anodization that results in a constant oxide δ_b at the pore bottom (time independent),[23,24] TiO_2 NTs present a nonsteady-state anodization that leads to the progressive increase of δ_b over time and limits the growth of NTs (because the ion diffusion path in the barrier extensively increases).[9,12,22,25−27]

However, it is usually stated that the final δ_b value of both anodic oxides, for long anodizations, is not considerably changed with time, but depends linearly (and exclusively) on the applied potential

$$\delta_b = kV \qquad (2)$$

where k is a proportionality constant, equal to 1.3 and 2.2 nm/ V for AAO and TiO_2 NTs, respectively.[21,24,28] However, other $\delta_b(V)$ dependencies were described.[29] Schultze et al. also reported that k in TiO_2 NTs depends slightly on the experimental conditions, particularly the anodization time.[3]

Following the metal oxidation theory of Cabrera and Mott,[1] the oxide initially grows very rapidly because the strong electric field ($E > 10^6$ V/cm) highly enhances ionic transport. However, as the oxidation proceeds, the increasing thickness of the oxide will slow ionic diffusion (longer pathway for ions to cross) and thus the oxide growth rate is limited. This gives rise to the logarithmic law

$$\frac{1}{\delta_b} = A - B\ln(t) \qquad (3)$$

where A and B are material- and temperature-dependent constants.

Several kinetic models of oxide growth for TiO_2 NTs have been reported, mostly concerning the influence of the anodization voltage,[20,21,29] but limited data were reported on the evolution of δ_b with time, and no model incorporating both anodization potential and time is available in the literature.

In this work we studied the effect of the anodization potential and time on the growth rate of the TiO_2 NTs barrier layer. We performed a systematic study on the electrochemical anodization of Ti under a wide range of applied potentials (20−80 V; at fixed anodization time) and time (0.5−72 h; at constant potential). A relation between the δ_b experimental data and the classical theoretical model of Cabrera and Mott is here established; we propose an equation ruling the growth of δ_b depending both on V and time [$\delta_b(V,t)$]. Our relation gives crucial information on the oxide growth phenomena occurring at the bottom of the NTs and allows us to predict the δ_b state at any anodization moment. By reaching a more concrete relationship than eq 2, we here provide a detailed description of k (usually described as a material constant).

The main mechanisms responsible for the NTs formation in Ti anodization processes are (a) electric-field-assisted oxidation at the metal/oxide interface, forming a TiO_2 layer, (b) field- assisted dissolution of the oxide layer (at the oxide/electrolyte interface), and (c) oxide chemical dissolution. While processes (a) and (b) occur at the bottom of the NTs, process (c) occurs at both, NTs top and bottom.[9,12,14,25,26] Differently from the Al valve metal anodization case, where a steady-state process is achieved, in the case of Ti anodization the NT parameters, mainly the length, are severely influenced by the additional chemical dissolution processes that occur at the NTs top and bottom.[14,29] In a steady-state anodization, the equilibrium between oxidation and dissolution processes at the pore bottom leads to a constant δ_b, while a nonsteady-state with higher oxidation than dissolution rates results in the progressive δ_b increase.[22]

Figures 1 and 2 show scanning transmission electron microscopy (STEM) images of the NTs barrier layer for 3 h anodizations under different V and for different anodization times under 60 V, respectively. In general, the NTs present similar morphologies, with a smooth structure and well-defined bottoms, characteristic of anodizations in ethylene-glycol-based electrolytes.[9,30] Only the 80 V sample presents a different NT morphology, typical of hard anodization conditions with very irregular shape, no smooth walls, and with ridges along them (Figure 1e). The STEM images allowed us to extract the δ_b values of both sets of samples. These measurements were carefully performed on the NTs bottom because the wall thickness varies along its length. In fact, the chemical dissolution process results in thinner NT walls and larger inner diameters at the NT tops (V-shape morphology).[31−33] The expected linear dependence on V is observed, with $\delta_b = 1.24V + 10.3$ for an anodization time of 3 h (Figure 3a). Indeed, the charge transfer during the anodization increases with increasing potential, enhancing oxidation over dissolution and resulting in a δ_b increase. Notice that even for the lowest potential (20 V; with δ_b = 34.39 nm) we are in the strong-field regime with $E = (V/\delta_b) \approx 5.81 \times 10^6$ V/cm, above the minimum field condition ($E > 10^6$ V/cm) assumed in the high- field conducting oxidation theory.[1] The results obtained with different anodization times (under V = 60 V) are presented in Figure 3b. Unlike AAO, where δ_b depends only on the applied potential,[24,34] in anodic titanium oxide, δ_b increases with time. In fact, we see an initially rapid

growth of δ_b (up to 3 h), followed by a slower growth, because the increase in δ_b decreases the ionic flow. Nevertheless, δ_b is still growing at 72 h, not reaching a stationary state as usually predicted. The δ_b growth with time, follows the logarithm relation $\delta_b = 74.4 + 5.42 \ln(t - 0.43)$. This progressive increase in δ_b indicates a nonsteady anodization evolution during the oxidation/dissolution processes (oxidation rate is higher than the dissolution) at the bottom of the NTs. Time is thus a crucial factor that cannot be neglected when modeling the growth of anodic δ_b, as occurred up to now.

In the Mott−Cabrera model, the rate-limiting step is the entry of cations (in our case Ti^{4+}) into the oxide from the metal. During oxidation, both the rate of oxidation and the rate- limiting process depend on the oxide thickness, giving the characteristic logarithmic growth law. In other words, the potentiostatic film growth is self-limiting as E is lowered with increasing film thickness. In this high-field conduction theory, the growth kinetics of the oxide film is described by j and related to the voltage drop across the oxide barrier by eq 1. The growth of δ_b is accompanied by an exponential decrease in j as E across the oxide continuously decreases.[1] When E is strong (>10^6 V/cm), the rate of oxidation is determined only by the rate at which ions leave the metal. In the case of an electrolyte-assisted oxidation (with O^{2-} anions), the growth rate of the anodic oxide film is given by

$$\frac{d\delta_b}{dt} = ue^{\delta_{b1}/\delta_b} = ue^{\beta E} \quad (4)$$

with

$$u = N'\Omega\nu e^{-W/k_B T} \quad (5)$$

and

$$\delta_{b1} = \frac{qa'V}{k_B T} = \beta V \quad (6)$$

where W is the activation energy for an ion to be removed from the metal surface (it then moves by field-assisted into an interstitial position of the oxide ($W \sim$ eV; see below)), N' is the number of ions at the metal interface per surface area (surface density of mobile defects; set to $1/a^2$, where a is the inter atomic distance of the oxide), Ω is the oxide volume per defect (set to a^3), and ν(~10^{12} s^{-1}) is the atomic frequency vibration of the oxide; we thus have $N'\Omega\nu \approx 10^{11}$ nm/s. a' is the hopping distance (relevant activation distance near the metal/oxide interface); $q = Ze$ is on the order of the effective defect charge (with Z and e as the cation and electron charges, respectively); k_B is the Boltzmann constant; and T the temperature ($k_B T$ = 0.025 eV at room temperature). Finally, u is the velocity at which the cation thermally escapes from the potential barrier to an interstitial position, that is, in the absence of E.[1] One assumes that the oxide growth is dominated by cation injection at defective sites that correspond to low-energy spots at the metal interface and is thus dominated by W. Equation 4 is valid only for $\delta_b \ll \delta_{b1}$ and shows that the growth rate is very large for small δ_b. A consequence of eq 4 is that for constant V and low T ($k_B T \ll W$), u is negligibly small and the oxide

grows up to a certain limiting thickness (δ_{bL}). For practical purposes, it is defined as δ_{bL} the oxide thickness that makes the growth rate ($d\delta_b/dt$) = 10^{-6} nm/s (about one atomic layer added in 10^5 s). With this condition and $N'\Omega v \approx 10^{11}$ nm/s inserted in eq 4 one has $\exp((\delta_{b1}/\delta_{bL}) - (W/k_BT)) = 10^{-17}$. Using now eq 6, δ_{bL} can be estimated[1]

$$\delta_{bL} = \frac{qa'V}{W - 39k_BT} = \beta' V \tag{7}$$

For higher temperatures (above $W/39k_B$) there is no limiting thickness and the initial rapid growth rate turns into a parabolic growth law.[1] Thus, growth is self-limiting as E is lowered with increasing δ_b. For $\delta_b \ll \delta_{b1}$, the integration of eq 4, neglecting terms higher than δ_b/δ_{b1}, leads to

$$\frac{\delta_{b1}}{\delta_b} = -\ln\left(\frac{\delta_{b1} u t}{\delta_{bL}^2}\right) \tag{8}$$

One notices that the δ_{b1}/δ_{bL} ratio is independent of V, q, and a', so that we can obtain W (using eqs 6 and 7) as

$$W = \left(\frac{\delta_{b1}}{\delta_{bL}} - 39\right) k_BT \tag{9}$$

From eq 8 we obtain the logarithmic growth law

$$\frac{1}{\delta_b} = A - B\ln(t) \tag{10}$$

with

$$A = \left[\ln\left(\frac{\beta'^2 V}{u\beta}\right)\right] \times \frac{1}{\beta V} \tag{11}$$

and

$$B = \frac{1}{\beta V} \tag{12}$$

Thus the ruling oxide growth equation as a function of V and t is given by

$$\frac{1}{\delta_b(V, t)} = \left[\ln\left(\frac{\beta'^2 V}{u\beta}\right)\frac{1}{\beta V} - \frac{1}{\beta V}\ln(t)\right] \tag{13}$$

The A and B parameters can be estimated using theoretical material-temperature-dependent quantities: u, δ_{b1}, and δ_{bL}. In the case of AAO (oxidation rate = dissolution rate; E and δ_b constant), all parameters are known and one has: $a = 0.4785$ nm, $v \approx 10^{12}$ s^{-1}, $W = 1.8$ eV, $a' = 0.35$ nm, and $k_BT = 0.025$ eV,[1] giving $u = 2.57 \times 10^{-20}$ nm·s^{-1}; $\delta_b = 42V$ ($\beta = 42$ nm·V^{-1}). For $V = 60$ V, we obtain $\delta_{b1} = 2250$ nm; $\delta_{bL} = 1.27V = 76.4$ nm. Replacing u, δ_{b1}, and δ_{bL} in eqs 11 and 12, we obtain the theoretical estimations (for 60 V): $A^T = 0.01823$ nm^{-1} and $B^T = 3.97 \times 10^{-4}$ nm^{-1}.

In the case of TiO_2 NTs formation by Ti anodization, the relevant oxide thickness growth is the NTs bottom barrier layer. Its growth rate is also limited by the migration of ionic species under the effect of a high applied electric field, where the movement of the Ti/TiO_2 interface involves the transport of metal cations (Ti^{4+}) in the direction of the electrolyte and the oxygen ions (and probably some incorporated anions) in the direction of the metal.[20,21] Under the high field model, δ_b depends on E (and V) according to eq 1, fostering faster ionic transport with higher potentials (interface reaction becomes rate-determining), as already discussed. In the AAO case the limiting δ_b value is reached when the oxide formation rate is equal to the dissolution rate,[21,23] while in TiO_2 NTs it increases with time. In the latter case, the lack of equilibrium between the dissolution and oxidation processes during the anodization turns time as a parameter to consider.[22]

Schultze et al. reported that the TiO_2 barrier layer growth has a rate parameter ($d\delta_b/dV$) with values between 1.3 and 3.3 nm·V^{-1} (depending on the anodization conditions) and the native oxide layer stands in the range $\delta_b^0 = 1.3-5.4$ nm.[3] In this context, our $\delta_b(V)$ experimental values, obtained from the STEM images of the 3 h anodized samples, showed that the linear fit (using the traditional eq 2) leads to a constant growth rate of $k = 1.24$ nm·V^{-1} with an intercept at $V = 0$ of $\delta_b^0 = 10.3$ nm, which is too large to be attributed to the stable native oxide layer. Therefore, by using the experimental data, we aim to fit the full equation behind $\delta_b(V,t)$ that comprehensibly describes the detailed growth dependencies.

Figure 4 shows the experimental data, considering $1/\delta_b$ for a constant potential ($V = 60$ V) with different anodization times. We can use the high-field Cabrera and Mott logarithmic growth law model (eq 10) to obtain the A (eq 11) and B (eq 12) experimental parameters. Plotting the experimental data as $1/\delta_b$ versus $\ln(t)$ (inset of Figure 4), we obtain a linear fit described by the equation

$$\frac{1}{\delta_b(t)} = 0.0128 - 5.96 \times 10^{-4} \times \ln(t - 0.43) \qquad (14)$$

One notices that the obtained A and B values are on the same order of magnitude with the estimated ones for the case of AAO ($A^T = 0.0182$ nm^{-1}, and $B^T = 3.97 \times 10^{-4}$ nm^{-1}). Introducing the obtained parameters A and B in eqs 11 and 12, respectively, we have

$$0.0128 = [\ln(cV)] \times \frac{1}{\beta V} \qquad (15)$$

$$5.96 \times 10^{-4} = \frac{1}{\beta V} \qquad (16)$$

where c is the $(\beta'^2/u\beta)$ ratio. Because V = 60 V, we obtain β = 27.98 nm·V^{-1} and c = 3.534 × 10^7 h·V^{-1}. Considering eq 13 in the form of eq 2 and the calculated A and B constants, we can model a relation between δ_b and V, t as

$$\delta_b(V, t) = \left[\frac{27.98}{\ln(3.53 \times 10^7 V) - \ln(t - 0.43)}\right] V \qquad (17)$$

Equation 17 describes the barrier layer thickness increase with V and t, giving the k corresponding dependency, $k = (27.98/(\ln[(3.53 \times 10^7 V) - \ln(t - 0.43)]))$ nm·V^{-1}. If we consider the same anodization time (t = 3 h) and different anodization potentials, 20 and 60 V, we obtain k = 1.43 and 1.36 nm·V^{-1}, respectively. If we now consider the same potential (60 V) but different anodization times, t = 3 and 72 h, we obtain k = 1.36 and 1.63 nm·V^{-1}, respectively. Thus, k stands as a variable parameter and not as a material constant as considered for AAO[24,28] and TiO_2 NTs[21] templates. Note that the obtained k is in the range of the reported ones (1.3−3.3 nm·V^{-1}).[3]

Figure 5 displays the δ_b values for different potentials extracted from the experimental STEM images, calculated using the $j(t)$ curves and eq 17 from our model (with β = 27.98 nm·V^{-1}, c = 3.534 × 10^7 h·V^{-1} and t = 3 h). The calculated $\delta_b(V,t)$ (eq 17) is remarkably close to the experimental data, with only a small deviation at low V values. Notice that eq 17 predicts a zero δ_b if no voltage is applied, discarding the presence of the thin native oxide layer present on the surface of the Ti metal.

Despite this, the final $\delta_b(V,t)$ is in good agreement with the Ti anodization experimental results in the considered working range, indicating the validity of the developed model.

From the obtained results we can now extract phenomeno- logical constants, a' and W. In fact, from eq 6 with β = 27.98 nm·V^{-1}, we obtain the hopping distance, a' = 0.1749 nm. From the ratio $c = (\beta'^2/u\beta)$, replacing β by eq 6, β' by eq 7, and u by eq 5, using the constant values (a' = 0.1749 nm, c = 3.534 × 10^7 h·V^{-1}) and solving the equation as a function of W, we obtain W = 0.98 eV. Additionally, taking into account eqs 6 and 7 for V = 60 V, one finds δ_{b1} = 1679 nm (which satisfies the condition imposed by the model, $\delta_{b1} \gg \delta_b$) and the limiting thickness, δ_{bL} = 8394 nm. A representative value of δ_{bL} should be obtained, in principle, under steady-state conditions, which is not the case of Ti anodization. Notice that using the ratio δ_{b1}/δ_{bL} in eq 9 we also obtain W = 0.98 eV, supporting the previous calculation.

During anodization, the evolution of the current density (j) with time is a direct indication of the oxide growth state, that is, NTs formation and growth. The 3 h anodization curves for the first set of samples featuring under V (from 20 to 80 V) are shown in Figure 6a. The time evolution of δ_b during

the anodization (Figure 6b) can be directly extracted from the $j(t)$ curves because one can rewrite eq 1 as

$$\delta_b = \frac{\beta V}{\ln\left(\frac{j}{\alpha}\right)} \quad (18)$$

$$\alpha = N' q \nu e^{(-W/k_B T)} \quad (19)$$

and

$$\beta = \frac{qa'}{k_B T} \quad (20)$$

where $\alpha = 4.2 \times 10^{-9}$ mA·cm^{-2} (using $W = 0.98$ eV) and $\beta = 27.98$ nm·V^{-1} for TiO_2 in the present anodization conditions. Using eq 18, the $\delta_b(t)$ values during the anodization for each potential are obtained (inset of Figure 6b). The Ti anodizations from 20 to 60 V present the typical initial current density transients for anodic NTs oxide (Figure 6): the sharp initial j decrease corresponds to the rapid (and continuous) oxide barrier formation, followed by a lower rate j decrease that marks the beginning of pore nucleation on the oxide topographic minima due to the field-assisted dissolution, until j minimum (j_{min}) is reached (maximum δ_b). Afterward, the pore formation arises, which is translated by a δ_b slight decrease until a minimum is seen (corresponding to j_{max}). From this point onward the NTs start to grow, but δ_b continues to slowly increase (inset of Figure 6b) as the anodization proceeds due to the out-balanced oxidation/dissolution processes characteristic of the Ti nonsteady-state anodization.[22] This is related to gradual failure of F^- ions (crucial for the dissolution process) at the electrolyte/TiO_2 interface, which are difficult to replace by new ones, giving the high viscosity of the electrolyte and the increasing NTs length (diffusion-limited process).[30] Therefore, the oxidation process is faster than the dissolution, resulting in the slowly δ_b increase (and j decrease) with time (Figure 6a,b).[22]

We notice that j increases with the applied potential in agreement with eq 1 because higher potentials induce larger driving forces for ionic migration.[1,12,15] The ionic current is directly related with the applied potential responsible for the field-enhanced oxidation and dissolution and thus to the processes responsible for oxide formation, pore nucleation and pore growth. Thus, increasing the electric field leads to higher growth rates. Up to 60 V one finds that pore nucleation j_{min} and j_{max} are steadily being reached sooner because 60 V is the most favorable regime for pore growth.

The $j(t)$ curves at higher potentials (70 and 80 V), besides being irregular with an oscillatory tendency, show a noticeable decrease over the whole anodization period with the absence of the nucleation stage, j_{min} and j_{max}. These $j(t)$ curves show the typical hard-anodization behavior, being indicative of much strong oxidation than dissolution throughout the anodization process.[15,35,36] With these conditions, the intense and much higher currents, resulting from a stronger ionic flow, lead to a more rapid increase of δ_b over time, extending the ionic diffusion path and preventing a balanced steady-state anodization. The nonhomogeneous field distribution over the sample due to the typical topography of a Ti foil should originate different anodization growth

rates, with the macroscopic $j(t)$ curve being the reflection of all anodization zones.[22] Finally, we were able to additionally calculate $\delta_b(V)$ using the anodization curves (Figure 5 red squares). To this end, $\delta_b(V)$ was obtained using eq 18 (with $\alpha = 4.2 \times 10^{-9}$ mA·cm^{-2}, $\beta = 27.98$ nm·V^{-1}) and the final $j(t)$ value (j_{final}) for each V anodization curves. Such values are in excellent agreement with the STEM data and the deduced model curve, reinforcing the validity of our calculations.

Up to now, TiO_2 NT reports have considered that, as in AAO, δ_b is constant with time. Our results show that because the oxidation and dissolution processes are not in equilibrium during the anodization of Ti, δ_b increases with time, and a more realistic and complete expression for δ_b was obtained. We then established a relationship between δ_b and the applied voltage and time [$\delta_b(V,t)$]. This implies that the growth constant k (until now considered only material-dependent) is also governed by the V and t anodization parameters. The theoretical model is in excellent agreement with the experimental data and can be used to predict the δ_b outcome for different anodization voltages and time.

EXPERIMENTAL SECTION

The electrochemical anodization of 1 × 1 cm^2 Ti foils (99.99+% high-purity from AlfaAesar, 0.127 mm) was performed. Prior to the anodization, the samples were ultrasonically cleaned sequentially with ethanol and deionized water (3 min). The Ti foil anodizations were performed using a homemade setup, consisting of a two-electrode anodization cell, with a platinum mesh used as the cathode and the Ti foil sample in contact with a copper cap used as the anode (anodization area of 0.196 cm^2). Anodizations were performed using a DC power supply Keithley model 2004 Sourcemeter, monitored and controlled by a LabView application. The electrolyte used was an ethylene glycol solution containing NH_4F (0.3 wt %) and H_2O (2 wt %), at room temperature, with magnetic stirring.[9,22] Two sets of anodized samples were prepared: (i) TiO_2 NTs with applied potentials ranging from 20 to 80 V (for 3 h) and (ii) TiO_2 NTs with anodization times ranging from 0.5 to 72 h (at an applied potential of 60 V). After the anodization, each sample was sequentially rinsed in ethanol, deionized water, and dried with a nitrogen stream. The TiO_2 NT template was then mechanically detached from the Ti foil, and their morphology was characterized by STEM technique (FEI Quanta 400FEG field emission scanning electron microscopy). This allowed us to determine δ_b at the bottom of the NTs using ImageJ open- source software.[37]

AUTHOR INFORMATION

Corresponding Author

*E-mail: jearaujo@fc.up.pt.

Notes

The authors declare no competing financial interest.

ACKNOWLEDGMENTS

This work was supported by the Portuguese Foundation for Science and Technology (FCT), under the project CERN/FP/ 123585/2011 and by the Associated Laboratory IN. A.A. acknowledges the financial support under project PTDC/ CTM-MET/118236/2010. C.T.S. is also grateful to FCT for the Post-Doc fellow (reference: SFRH/BPD/82010/2011). J.V. acknowledges financial support

through FSE/POPH.

REFERENCES

(1) Cabrera, N.; Mott, N. F. Theory of the Oxidation of Metals. *Rep. Prog. Phys.* 1949, *12*, 163−184.

(2) Schultze, J. W.; Lohrengel, M. M.; Ross, D. Nucleation and Growth of Anodic Oxide Films. *Electrochim. Acta* 1983, *28*, 973−984.

(3) Schultze, J. W.; Lohrengel, M. M. Stability, Reactivity and Breakdown of Passive Films. Problems of Recent and Future Research. *Electrochim. Acta* 2000, *45*, 2499−2513.

(4) Hebert, K. R.; Albu, S. P.; Paramasivam, I.; Schmuki, P. Morphological Instability Leading to Formation of Porous Anodic Oxide Films. *Nat. Mater.* 2012, *11*, 162−166.

(5) Sousa, C. T.; Leitao, D. C.; Proenca, M. P.; Ventura, J.; Pereira, A. M.; Araujo, J. P. Nanoporous Alumina as Templates for Multifunc- tional Applications. *Appl. Phys. Rev.* 2014, *1*, 031102.

(6) Grätzel, M. Photoelectrochemical Cells. *Nature* 2001, 414−338.

(7) O′Regan, B.; Grätzel, M. A Low-Cost, High Efficiency Solar Cell Based on Dye-Sensitized Colloidal TiO_2 Films. *Nature* 1991, 737− 740.

(8) Krüger, J.; Plass, R.; Grätzel, M.; Matthieu, H.-J. Improvement of the Photovoltaic Performance of Solid-State Dye-Sensitized Device by Silver Complexation of the Sensitizer Cis-Bis(4,4-dicarboxy-2,2bipyridine)-Bis(isothiocyanato) Ruthenium(II). *Appl. Phys. Lett.* 2002, *81*, 367−369.

(9) Shankar, K.; Mor, G. K.; Prakasam, H. E.; Yoriya, S.; Paulose, M.; Varghese, O. K.; Grimes, C. A. Highly-Ordered TiO_2 Nanotube Arrays up to 220 μm in Length: Use in Water Photoelectrolysis and Dye- Sensitized Solar Cells. *Nanotechnology* 2007, *18*, 065707.

(10) Zwilling, V.; Aucouturier, M.; Darque-Ceretti, E. Anodic Oxidation of Titanium and TA6V Alloy in Chromic Media. An Electrochemical Approach. *Electrochim. Acta* 1999, *45*, 921929.

(11) Mor, G. K.; Varghese, O. K.; Paulose, M.; Shankar, K.; Grimes, C. A. A Review on Highly Ordered, Vertically Oriented TiO_2 Nanotube Arrays: Fabrication, Material Properties, and Solar Energy Applications. *Sol. Energy Mater. Sol. Cells* 2006, *90*, 2011−2075.

(12) Sun, L.; Zhang, S.; Sun, X. W.; He, X. Effect of Electric Field Strength on the Length of Anodized Titania Nanotube Arrays. *J. Electroanal. Chem.* 2009, *637*, 6−12.

(13) Mor, G. K.; Shankar, K.; Paulose, M.; Varghese, O. K.; Grimes, C. A. Enhanced Photocleavage of Water Using Titania Nanotube Arrays. *Nano Lett.* 2005, *5*, 191−195.

(14) Macák, J. M.; Tsuchiya, H.; Schmuki, P. High-Aspect-Ratio TiO_2 Nanotubes by Anodization of Titanium. *Angew. Chem., Int. Ed.* 2005, *44*, 2100−2102.

(15) Sulka, G. D.; Kapusta-Koodziej, J.; Brzoźka, A.; Jaskua, M. Fabrication of Nanoporous TiO_2 by Electrochemical Anodization. *Electrochim. Acta* 2010, *55*, 4359−4367.

(16) Gong, D.; Grimes, C. A.; Varghese, O. K.; Hu, W.; Singh, R. S.; Chen, Z.; Dickey, E. C. Titanium Oxide Nanotube Arrays Prepared by Anodic Oxidation. *J. Mater. Res.* 2001, *16*, 3331−3334.

(17) Vega, V.; Cerdeira, M. A.; Pride, V. M.; Alberts, D.; Bordel, N.; Pereiro, R.; Mera, F. F.; Garcia,

S.; Hernandez-Velez, M.; Vasquez, M. Electrolyte Influence on the Anodic Synthesis of TiO_2 Nanotube Arrays. *J. Non-Cryst. Solids* 2008, *354*, 52335235.

(18) Tang, X.; Li, D. Fabrication, Geometry, and Mechanical Properties of Highly Ordered TiO_2 Nanotubular Arrays. *J. Phys. Chem. C* 2009, *113*, 7107−7113.

(19) Berger, S.; Kunze, J.; Schmuki, P.; LeClere, D.; Valota, A. T.; Skeldon, P.; Thompson, G. E. A Lithographic Approach to Determine Volume Expansion Factors During Anodization: Using the Example of Initiation and Growth of TiO_2-Nanotubes. *Electrochim. Acta* 2009, *54*, 5942−5948.

(20) Prakasam, H. E.; Shankar, K.; Paulose, M.; Varghese, O. K.; Grimes, C. A. A New Benchmark for TiO_2 Nanotube Array Growth by Anodization. *J. Phys. Chem. C* 2007, *111*, 7235−7241.

(21) Macak, J. M.; Hildebrand, H.; Marten-Jahns, U.; Schmuki, P. Mechanistic Aspects and Growth of Large Diameter Self-Organized TiO_2 Nanotubes. *J. Electroanal. Chem.* 2008, *621*, 254−266.

(22) Apolinário, A.; Sousa, C. T.; Ventura, J.; Costa, J. D.; Leitão, D. C.; Moreira, J. M.; Sousa, J. B.; Andrade, L.; Mendes, A. M.; Araújo, J. P. The Role of the Ti Surface Roughness in the Self-Ordering of TiO_2 Nanotubes: A Detailed Study of the Growth Mechanism. *J. Mater. Chem. A* 2014, *2*, 9067−9078.

(23) Parkhutik, V. P.; Shershulsky, V. I. Theoretical Modelling of Porous Oxide Growth on Aluminium. *J. Phys. D: Appl. Phys.* 1992, *25*, 1258−1263.

(24) Nielsch, K.; Choi, J.; Schwirn, K.; Wehrspohn, R. B.; Gösele, U. Self-Ordering Regimes of Porous Alumina: The 10 Porosity Rule. *Nano Lett.* 2002, *2*, 677−680.

(25) Sobieszczyk, S. Self-Organized Nanotubular Oxide Layers on Ti and Ti Alloys. *Adv. Mater. Sci. (Warsaw, Poland)* 2009, *9*, 14−17.

(26) Cai, Q. Y.; Paulose, M.; Varghese, O. K.; Grimes, C. A. The Effect of Electrolyte Composition on the Fabrication of Self-Organized Titanium Oxide Nanotube Arrays by Anodic Oxidation. *J. Mater. Res.* 2005, *20*, 230−236.

(27) Apolinário, A.; Sousa, C. T.; Ventura, J.; Andrade, L.; Mendes, A. M.; Araújo, J. P. Tailoring the Ti Surface via Electropolishing Nanopatterning as a Route to Obtain Highly Ordered TiO_2 Nanotubes. *Nanotechnology* 2014, *25*, 485301.

(28) Sousa, C. T.; Leitão, D. C.; Proença, M. P.; Apolinário, A.; Correia, J. G.; Ventura, J.; Araújo, J. P. Tunning Pore Filling of Anodic Alumina Templates by Accurate Control of the Bottom Barrier Layer Thickness. *Nanotechnology* 2011, *22*, 315602.

(29) Su, Z.; Zhou, W. Formation, Microstructures and Crystallization of Anodic Titanium Oxide Tubular Arrays. *J. Mater. Chem.* 2009, *19*, 2301.

(30) Sreekantan, S.; Saharudin, K. A.; Lockman, Z.; Tzu, T. W. Fast Rate Formation of TiO_2 Nanotube Arrays in an Organic Bath and their Applications in Photocatalysis. *Nanotechnology* 2010, *21*, 365603.

(31) Macak, J. M.; Tsuchiya, H.; Ghicov, A.; Yasuda, K.; Hahn, R.; Bauer, S. TiO_2 Nanotubes: Self-Organized Electrochemical Formation, Properties and Applications. *Curr. Opin. Solid State Mater. Sci.* 2007, *11*, 3−18.

(32) Yuan, X.; Zheng, M.; Ma, L.; Shen, W. High-Speed Growth of TiO_2 Nanotube Arrays With

Gradient Pore Diameter and Ultrathin Tube Wall under High-Field Anodization. *Nanotechnology* 2010, *21*, 405302.

(33) Su, Z.; Zhou, W. Pore Diameter Control in Anodic Titanium and Aluminium Oxides. *J. Mater. Chem.* 2011, *21*, 357−362.

(34) Sulka, G. D.; Stpniowski, W. J. Structural Features of Self-Organized Nanopore Arrays Formed by Anodization of Aluminum in Oxalic Acid at Relatively High Temperatures. *Electrochim. Acta* 2009, *54*, 3683−3691.

(35) Lee, W.; Ji, R.; Gösele, U.; Nielsch, K. Fast Fabrication of Long-Range Ordered Porous Alumina Membranes by Hard Anodization. *Nat. Mater.* 2006, *5*, 741−747.

(36) Choi, J.; Wehrspohn, R. B.; Lee, J.; Gösele, U. Anodization of Nanoimprinted Titanium: a Comparison with Formation of Porous Alumina. *Electrochim. Acta* 2004, *49*, 2645−2652.

(37) Rasband, W. S. *ImageJ*; U. S. National Institutes of Health: Bethesda, MD, 1997−2014. http://rsb.info.nih.gov/ij/.

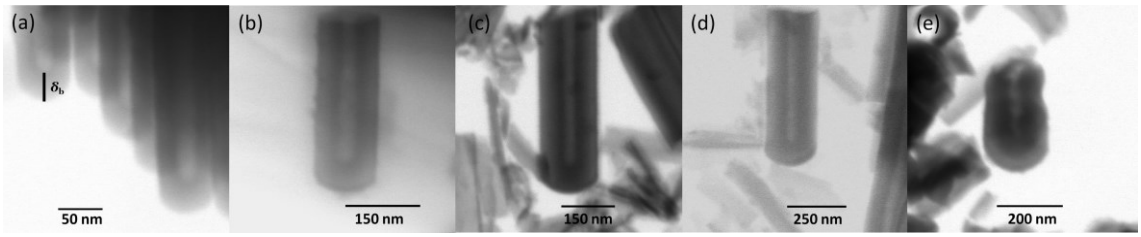

Figure 1. STEM images of TiO_2 NT bottoms and respective measurements of the barrier layer thickness (δ_b) of samples anodized for 3 h under different potentials: (a) 20, (b) 40, (c) 60; (d) 70, and (e) 80 V

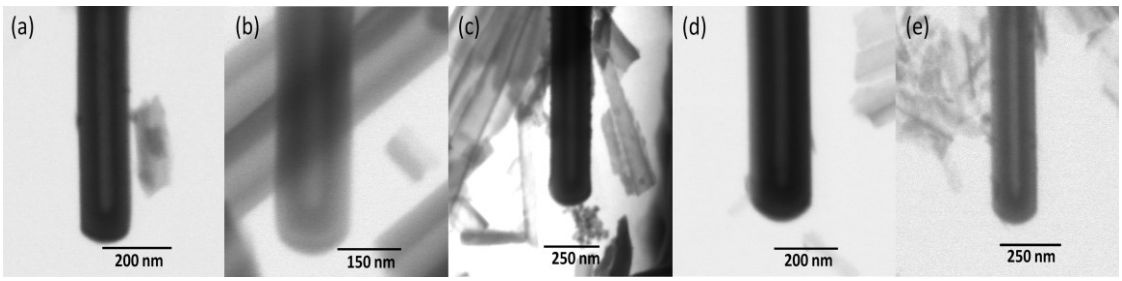

Figure 2. STEM images of TiO_2 NT bottoms and respective measurements of the barrier layer thickness (δ_b) of samples anodized under 60 V and different anodization time: (a) 1, (b) 5, (c) 10, (d) 24, and (e) 72 h.

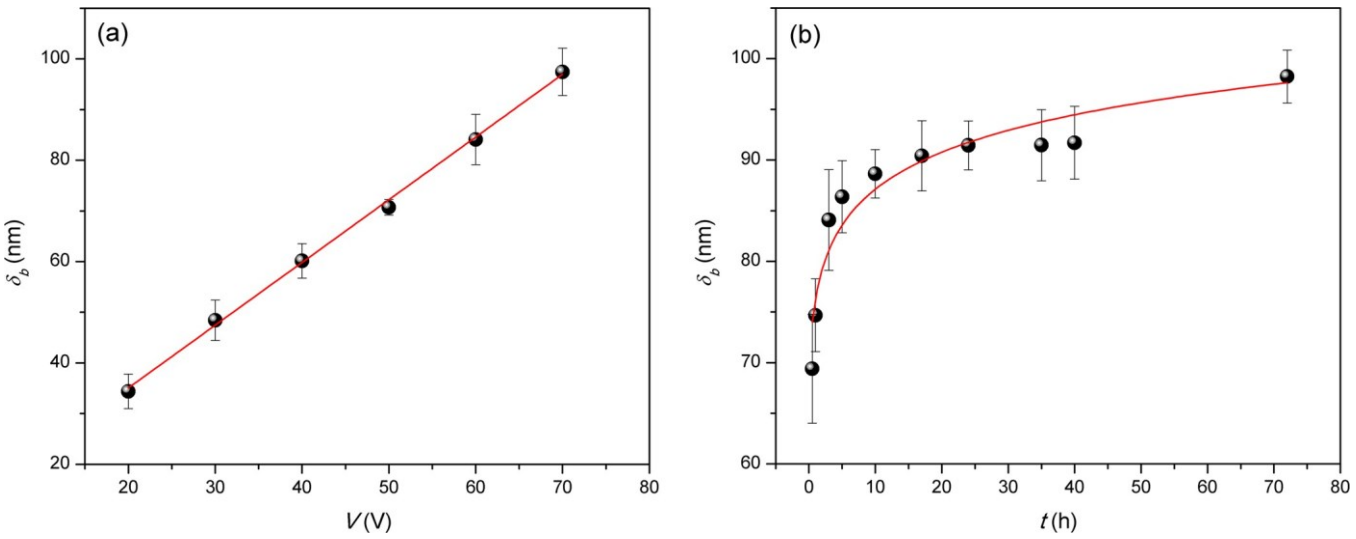

Figure 3. Evolution of barrier layer thickness (δ_b) in TiO_2 nanotubes as a function of (a) potential (V; with constant anodization time of t = 3 h), showing a linear dependency on V (correlation parameter estimated from the linear regression is $k = 1.24\ \text{nm}\cdot\text{V}^{-1}$), and (b) anodization time (t; with a constant anodization potential of V = 60 V), showing a logarithmic growth with t.

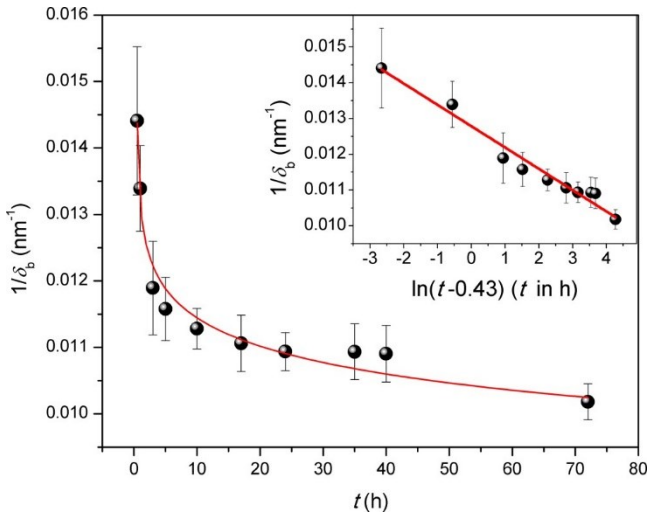

Figure 4. Inverse of δ_b as a function of anodization time (t) for V = 60 V and corresponding fit with the high-field Cabrera and Mott logarithmic growth law model (eq 10). Inset shows the linear fit of $1/\delta_b$ versus ln (t).

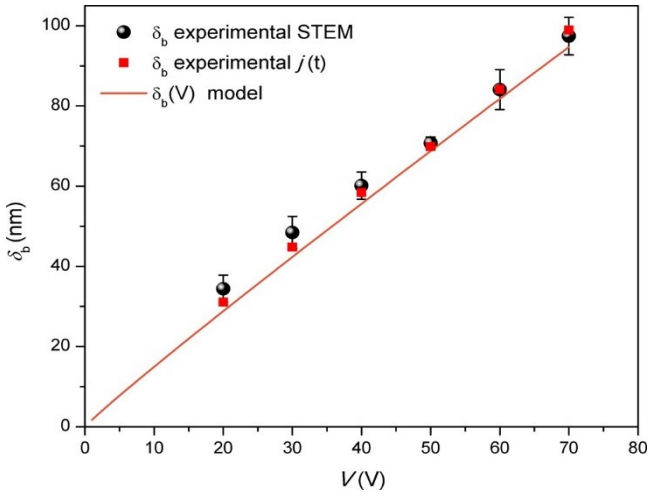

Figure 5. Barrier layer thickness (δ_b) values for different potentials obtained from the STEM measurements, from the model (eq 17) and from the $j(t)$ curves.

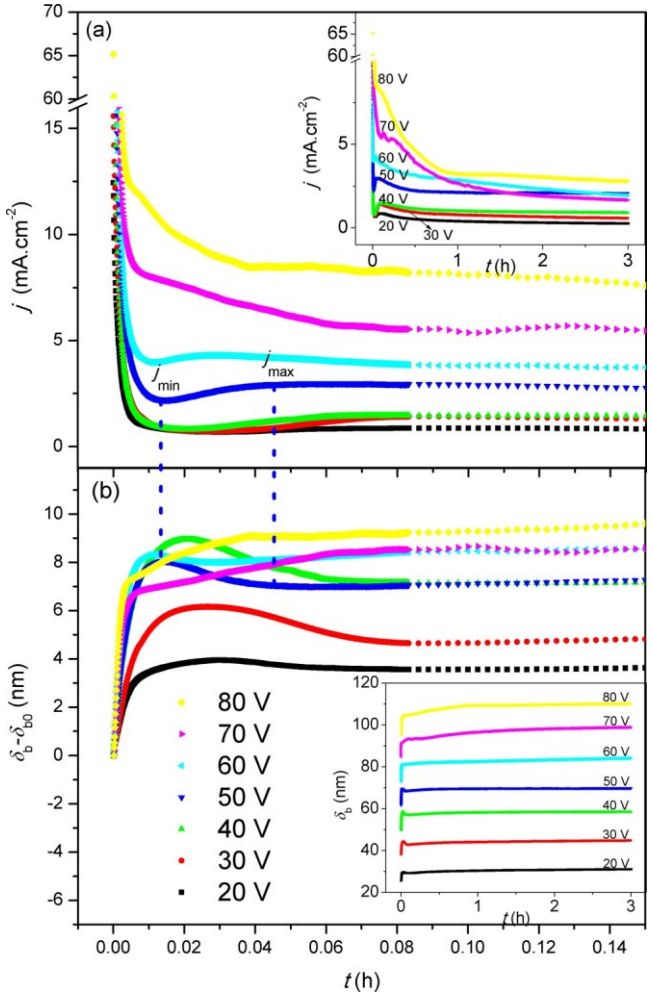

Figure 6. (a) Current density $j(t)$ anodization curves. (b) TiO_2 barrier layer thickness $\delta_b(t)$; curves during anodization time, for samples anodized with a potential range from 20 to 80 V. The first 8 min are presented (normalization of the δ_b transient period to compare with $j(t)$ transient period). The insets represent the complete anodization time (3 h).